Vectorially Oriented Monolayers of the Cytochrome *c*/Cytochrome Oxidase Bimolecular Complex

Ann M. Edwards,* J. Kent Blasie,* and John C. Bean#

*Department of Chemistry, University of Pennsylvania, Philadelphia, Pennsylvania 19104, and #Bell Laboratories/Lucent Technologies, Murray Hill, New Jersey 07974 USA

ABSTRACT Vectorially oriented monolayers of yeast cytochrome *c* and its bimolecular complex with bovine heart cytochrome *c* oxidase have been formed by self-assembly from solution. Both quartz and Ge/Si multilayer substrates were chemical vapor deposited with an amine-terminated alkylsiloxane monolayer that was then reacted with a hetero-bifunctional cross-linking reagent, and the resulting maleimide endgroup surface then provided for covalent interactions with the naturally occurring single surface cysteine 102 of the yeast cytochrome *c*. The bimolecular complex was formed by further incubating these cytochrome *c* monolayers in detergent-solubilized cytochrome oxidase. The sequential formation of such monolayers and the vectorially oriented nature of the cytochrome oxidase was studied via meridional x-ray diffraction, which directly provided electron density profiles of the protein(s) along the axis normal to the substrate plane. The nature of these profiles is consistent with previous work performed on vectorially oriented monolayers of either cytochrome *c* or cytochrome oxidase alone. Furthermore, optical spectroscopy has indicated that the rate of binding of cytochrome oxidase to the cytochrome *c* monolayer is an order of magnitude faster than the binding of cytochrome oxidase to an amine-terminated surface that was meant to mimic the ring of lysine residues around the heme edge of cytochrome *c*, which are known to be involved in the binding of this protein to cytochrome oxidase.

INTRODUCTION

Single monolayers of fully functional electron transport membrane proteins, or supramolecular complexes thereof, vectorially oriented on the surface of solid substrates have the potential to provide definitive information concerning the mechanism of their biological electron and ion transport function. This potential derives from the possibility to both control the state of the protein redox centers (e.g., electrochemically) and simultaneously determine key features of the protein structure (e.g., relative positions/orientations of redox centers) for this particular form of these proteins. In addition, the designed fabrication of such monolayer systems allows the exploration of the utility of these proteins, or specifically designed models thereof (Robertson et al., 1994; Rabanal et al., 1996), in tailoring the macroscopic electro-optical response of the substrate surface.

We have demonstrated via structural studies the ability to vectorially orient both peripheral membrane proteins and detergent-solubilized integral membrane proteins at the soft interface between an aqueous medium and the endgroups of an organic self-assembled monolayer (SAM) chemisorbed onto the surface of a solid substrate by employing designed specific interactions between particular residues on the protein's surface and the SAM's endgroups (Chupa et al., 1994). Although other research groups have focused on measurements of the functional aspects of such (or closely related, e.g., Langmuir-Blodgett) monolayer systems that were not structurally characterized (Song et al., 1993; Cullinson et al., 1994; Owaku et al., 1995; Jiang et al., 1996; Guo et al., 1996), we have focused instead on developing the physical techniques essential to determining the key structural features of the proteins within such vectorially oriented single monolayers. To date, this work has concerned the determination of the so-called profile structures of such monolayers uniquely and to a resolution of ~7 Å by x-ray interferometry/holography (Blasie et al., 1992; Chupa et al., 1994) which is essential to the verification of the monolayer assembly process including the protein vectorial orientation, the positions of the protein metal redox centers within this profile structure by resonance x-ray diffraction to within ±1–3 Å (Pachence et al., 1989), and the orientations of the redox centers within the monolayer structure by polarized x-ray spectroscopy (Zhang et al., 1997) and optical linear dichroism (Pachence et al., 1990). These techniques have recently been successfully applied to vectorially oriented monolayers of both cytochrome *c* covalently tethered to thiol SAM endgroups (Chupa et al., 1994) and detergent-solubilized cytochrome oxidase electrostatically tethered to amine SAM endgroups (Edwards et al., 1997). Cyclic voltammetry studies performed by others on similar, but structurally uncharacterized, supposedly monolayer, systems containing cytochrome *c* (Collinson at al., 1992) and cytochrome oxidase (Cullinson et al., 1994) nevertheless indicate that these membrane protein systems are fully functional.

In this work, we have extended our structural studies to single monolayers of yeast cytochrome *c* and its bimolecular complex with detergent-solubilized bovine heart cyto-

Received for publication 31 October 1996 and in final form 25 November 1997.

Address reprint requests to Dr. Ann M. Edwards, Department of Chemistry, University of Pennsylvania, Box 297, 231 S. 34th Street, Philadelphia, PA 19104-6323. Tel.: 215-573-7995; Fax: 215-573-2112; E-mail: edwards@jkb3.chem.upenn.edu.

0006-3495/98/03/1346/12 $2.00

chrome *c* oxidase. We observe profile structures for the component proteins qualitatively similar to those previously obtained but note that the rate of binding of cytochrome oxidase to the cytochrome *c* is an order of magnitude faster than the binding of cytochrome oxidase to an amine-terminated SAM. The spontaneous binding of cytochrome oxidase to its electron donor may produce a more natural model system for the study of electron transport phenomena than achieved by the cross-linking of these two proteins via protein modification (Zaslavsky et al., 1995; Malatesta et al., 1996), and these vectorially oriented monolayers of the bimolecular complex are now sufficiently well structurally characterized to undertake a number of such related functional studies.

MATERIALS AND METHODS

The Ge/Si multilayer substrates utilized in the x-ray diffraction experiments were fabricated by molecular beam epitaxy (MBE) at Bell Laboratories. Four-inch-diameter, p-type Si(100) wafers (SEH-America, Vancouver, WA) with a resistivity of 20 ohm cm were smoothed with 30 atomic monolayers of silicon (i.e., Si_{30}) before deposition of the two unit cell superlattice structure of the form $2(Ge_2Si_{30})$. Details of the MBE deposition procedures are given elsewhere (Bean et al., 1984). The use of only two unit cells in this inorganic reference structure provides continuous meridional x-ray diffraction over a wide range of q_z (the reciprocal space axis perpendicular to the substrate plane) and, hence, guarantees the maximal amount of interference with the scattering from the unknown organic/bio-organic overlayers to be attached later (Cowley, 1981). Furthermore, the more electron-dense Ge layers of the MBE substrates were chosen to be very thin to provide considerably more intense x-ray diffraction out to larger q_z than was previously obtained using substrates fabricated by magnetron sputtering (Amador et al., 1993; Xu et al., 1991). The wafers were cut with a diamond pencil to obtain 1 cm $\times$ 2 cm $\times$ 0.5 mm substrates. The 1-mm-thick quartz substrates (Esco products, Oak Ridge, NJ) used in the optical spectroscopy were also cut to 1 cm $\times$ 2 cm.

The organic compound 3-aminopropyltrimethoxysilane was purchased from Gelest (Tullytown, PA) and used without further purification. Self-assembled monolayers (SAMs) of this compound were formed on the surfaces of both quartz and Si/Ge multilayer substrates using a vacuum chemical vapor deposition apparatus and procedure similar to that outlined by Hong et al. (1994). Before deposition, the substrates were sonicated for 10 min in each of the following: methanol, chloroform, acetone (all HPLC grade, Fisher Scientific, Pittsburgh, PA) and nitric acid (certified ACS plus grade, Fisher Scientific, Pittsburgh, PA). The substrates were then rinsed well with ultrapure water (Millipore Corp., Bedford, MA) and dried with filtered nitrogen before loading them into the vacuum chamber. Before the vacuum deposition, the base pressure of the apparatus was $<$25 mTorr. During the approximately 10-h silane vapor deposition, the substrates were held at $\sim$90°C. After silane deposition, the substrates were annealed overnight in the vacuum chamber at approximately 155°C.

After cooling, the deposition system was vented with dry nitrogen and the SAM-coated substrates were immediately immersed in a 2 mM solution of the hetero-bifunctional cross-linker *N*-succinimidyl 6-maleimidocaproate (EMCS; Fluka Chemical Corp., St. Louis, MO) in absolute ethanol under argon. After 8 h, the substrates were removed and rinsed four times in fresh ethanol and then either stored in ethanol for up to 3 days or further rinsed in ultrapure water and then 1 mM TRIS (Sigma Chemical Co., St. Louis, MO), pH 8.0. The surface was then ready for introduction to a 15 μM solution of cytochrome *c* from *Saccharomyces cerevisiae* (Sigma) in 1 mM TRIS, pH 8.0. All solutions used in the preparation and study of these samples were made with ultrapure water unless otherwise stated. The coated substrates were incubated for 18–24 h in the yeast cytochrome *c* solution and then removed and rinsed in 1 mM TRIS, pH 8.0, until no more protein could be removed, as determined via optical absorption spectroscopy (see below). This rinsing procedure removed the majority of nonspecifically bound protein. The samples were then placed in 1 mM dithiothreitol (Sigma) for 5 min to remove the remainder of the nonspecifically bound protein suspected to be yeast cytochrome *c* dimers formed via a disulfide linkage between the single surface cysteine 102 residues of each monomer.

After another rinsing in 1 mM TRIS buffer, the cytochrome *c* monolayers were ready for study before subsequent incubation in the second protein, cytochrome *c* oxidase. This integral membrane protein was isolated and purified from beef heart mitochondria using further modifications of the method of Yonetani et al. (Okunuki et al., 1958; Yonetani et al., 1960) as described elsewhere (Edwards et al., 1997). To produce the bimolecular complex monolayer samples, the cytochrome *c* monolayers were incubated for 3–4 h in solutions of approximately 6 μM cytochrome oxidase in 0.1% *n*-dodecyl β-D-maltoside (Sigma) in 1 mM KPO_4 (Sigma), pH 7.4. Before further study, each specimen was removed from the oxidase solution and rinsed repeatedly with a detergent buffer solution of 0.1% *n*-dodecyl β-D-maltoside in 1 mM KPO_4, pH 7.4, until no more protein could be removed, as determined via optical absorption spectroscopy (see below).

Optical absorption spectra were recorded on the quartz/SAM/linker/protein specimens using a double-beam spectrophotometer (Hitachi model U2000, San Jose, CA). Cleaned, blank quartz was used for the baseline scan and in the reference position, and both the blank and the protein samples were placed with the normal to their plane at 45° to the incident beam inside quartz cuvettes (1 cm path length). The cuvettes were filled with either 1 mM TRIS, pH 8.0, or 0.1% *n*-dodecyl β-D-maltoside in 1 mM KPO_4, pH 7.4, to record the oxidized spectra, and several grains of sodium dithionite (Sigma) were added to obtain the reduced absorption spectra.

Meridional x-ray diffraction data as a function of q_z (where $q_z = (2 \sin \theta)/\lambda$, which corresponds to elastic photon momentum transfer parallel to the *z* axis, i.e., perpendicular to the substrate plane) was collected after each overlayer was added to the Ge/Si multilayer substrates, having already collected analogous data from the bare substrates. This meridional x-ray diffraction arises from the projection onto the *z* axis of the three-dimensional electron density distribution of the multilayer specimen along radial vectors perpendicular to the *z* axis. This projection is defined as the electron density profile, $\rho(z)$, for the multilayer specimen. The incident x-ray beam defines an angle ω with the substrate plane (*xy*), with meridional x-ray diffraction being observed for ω equal to θ, where 2θ is the angle between the incident and scattered beams.

The specimens were positioned on the ϕ axis of a Huber four-circle diffractometer that was oscillated over an appropriate range of ω values. This geometry enabled collection of meridional x-ray diffraction data with a two-dimensional, position-sensitive detector (Siemens Instruments, Madison, WI), which was mounted on the 2θ axis and interfaced to a GPXII Micro VAX computer (Digital Equipment Corp., Marlboro, MA). An Elliott GX-13 rotating anode x-ray generator (Enraf-Nonius, Bohemia, NY) operating at a target loading of 27 kW/mm^2 was used to produce the incident Cu emission spectrum. The $CuK_{\alpha 1}$ line (λ = 1.541 Å) was selected with a 37 mm $\times$ 20 mm cylindrically bent Ge(111) monochromator crystal (Innovative Technology, South Hamilton, MA) to produce a line-focused x-ray beam parallel to the ω axis. The specimen-to-detector distance was 350 mm, and the beam height was $\sim$6 mm at the specimen. The incident and scattered beams were in a dry helium atmosphere. The focused x-ray beam width at the detector and the spatial resolution of the two-dimensional, position-sensitive detector resulted in a Δq_z resolution of $\sim$0.001 Å^{-1}.

Throughout data collection, the bare Ge/Si multilayer substrates and those coated with the amine-terminated SAMs or EMCS linker were housed in an aluminum chamber with Saran (polyvinylidene chloride) windows (Goodfellow Corp., Cambridge, UK) in a dry helium atmosphere at room temperature (20 $\pm$ 0.5°C). The protein-coated specimens were housed in the same specimen chamber and maintained at 3–7°C and a constant relative humidity (98 $\pm$ 1%) with a humidity controller (Asturias et al., 1994). This humidity controller constantly circulated moist helium

through the specimen chamber to maintain the hydration of the protein samples.

Meridional x-ray diffraction patterns were collected in sequential 35-min time frames over an approximately 17-h time period and stored as two-dimensional data files. Each individual two-dimensional data file was integrated perpendicular to the q_z axis over the length of the line-focused x-ray beam, producing a one-dimensional data file (i.e., the number of x-ray counts versus detector channel number along the q_z axis). These one-dimensional data files were first examined for possible radiation damage or specimen instability over the course of data collection. No evolution of the meridional x-ray diffraction from the specimens over the total data collection time was evident. The two-dimensional data files themselves were then summed and corrected for any detector nonuniformities by employing a correction algorithm based on a two-dimensional data file obtained from uniform illumination of the detector with an ^{55}Fe source. These summed and corrected files were then similarly integrated (see above) to produce one-dimensional data files, which were transferred to a Silicon Graphics IRIS Indigo computer (Silicon Graphics, Mountain View, CA) for further analysis.

RESULTS

Amine-terminated SAM/EMCS/cytochrome *c*/cytochrome oxidase specimens were formed on quartz substrates for use in optical absorption measurements, which were performed both before and after the cytochrome oxidase incubation. Several different soaking times were investigated at both the cytochrome *c* and cytochrome oxidase incubation steps. The absorbances in the Soret regions of both the cytochrome *c* and cytochrome oxidase seemed to be optimized by incubating the SAM/EMCS-coated substrates in cytochrome *c* for approximately 24 h and then in cytochrome oxidase for just 3–4 h. Specimens on quartz substrates were prepared identically and simultaneously with those on the Ge/Si multilayer substrates so that the optical absorption spectra could be compared with the derived electron density profiles. Fig. 1 shows the optical absorption spectra of a sample, formed on quartz simultaneously with that prepared on a Ge/Si multilayer for the diffraction study below, both before (lower trace) and after (upper trace) incubation on the cytochrome oxidase. In these oxidized spectra, the contribution from the cytochrome oxidase can clearly be seen in the appearance of an additional peak at 280 nm in the upper trace. Because the oxidized Soret peaks (at 410 and 422 nm for cytochrome *c* and cytochrome oxidase, respectively) are too close to be easily resolved, the sample was reduced with sodium dithionite to better resolve the Soret peaks (416 nm for the cytochrome *c* and 443.5 nm for the cytochrome oxidase), and absorbances in the reduced Soret bands were used to estimate the relative concentrations of the proteins on each specimen's surface using the extinction coefficients for solutions given by Dickinson and Chien (1975) and Yonetani (1961). For the sample shown in Fig. 1, the reduced Soret bands of the bimolecular complex yielded surface concentrations for the cytochrome *c* and cytochrome oxidase of 30.0 and 5.6 nM, respectively. These values are consistent with approximately monolayer coverage in each case, although they alone cannot demonstrate such (see Discussion). In addition, incubation time studies indicated that the rate of binding of cytochrome oxidase to the cytochrome *c* is more than an order of magnitude (namely ~25 times) faster than the binding of the oxidase to an amine-terminated SAM surface. This indicates that cytochrome oxidase's binding specificity is much higher for the cytochrome *c* surface than for a planar monolayer of primary amine endgroups.

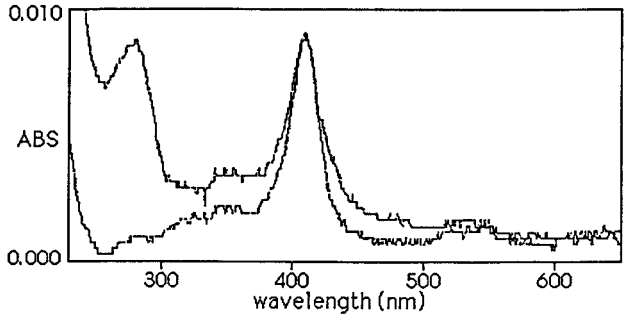

FIGURE 1 Optical absorption spectra of oxidized cytochrome *c* self-assembled onto quartz substrates that had been coated with an amine-terminated SAM and the hetero-bifunctional cross-linker, EMCS, before (*lower trace*) and after (*upper trace*) incubation in cytochrome oxidase.

The meridional x-ray scattering data for a typical bare Ge/Si multilayer substrate and for the same substrate/amine-terminated SAM/EMCS with just self-assembled cytochrome *c* bound, and then with both cytochrome *c* and cytochrome oxidase bound, are shown in Fig. 2 as $\log[I(q_z)]$. The data at higher q_z have been expanded 10-fold

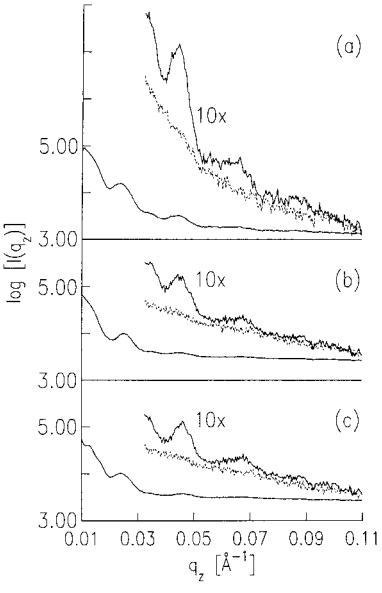

FIGURE 2 Meridional x-ray diffraction data, $\log[I(q_z)]$, for (*a*) a typical bare two-unit cell Ge/Si multilayer substrate and (*b*) for the same substrate plus amine-terminated SAM/EMCS linker with self-assembled cytochrome *c* covalently tethered to the surface and then (*c*) with cytochrome oxidase self-assembled onto the cytochrome *c*. The diffraction data at higher q_z are also shown on an expanded scale, along with the diffuse scattering measured in the plane of the Ewald sphere as described for each of these specimens. The abscissa is the reciprocal space coordinate, q_z ($Å^{-1}$), and the ordinate is the logarithm of counts collected.

to display the scattering more clearly. The absolute electron density profile, $\rho_{abs}(z)$, for these specimens can be expressed as shown in Eq. 1:

$$\rho_{abs}(z) = \bar{\rho}(z) + \Delta\rho(z), \quad (1)$$

where $\bar{\rho}(z)$ is the mean electron density profile and $\Delta\rho(z)$ is the electron density contrast profile, or the fluctuations about the mean electron density. The mean electron density profile gives rise to the specular x-ray scattering from the specimen's surface in the dynamical diffraction limit, especially for $q_z \leq (q_z)_{crit}$, whereas the electron density contrast profile gives rise to the kinematical meridional x-ray diffraction over all values of q_z (Blasie et al., 1992; Xu et al., 1993; Murphy et al., 1993). As we were primarily concerned with the kinematical diffraction within these data, the ω oscillations were, therefore, not extended down to the critical angle for specular scattering from the specimen's surface but were instead stopped at the equivalent reciprocal space $(q_z)_{min} \approx 0.01$ Å^{-1}. For the specimens studied, meridional x-ray scattering with a signal-to-noise ratio above background levels was generally observed out to $(q_z)_{max} \approx 0.08$ Å^{-1}.

The total meridional x-ray scattering, $I(q_z)$, arising from the absolute electron density profile, is shown in Eq. 2:

$$I(q_z) = |F_{tot}(q_z)|^2 = |F_{spec}(q_z)|^2 + |F_{kin}(q_z)|^2 + 2F_{spec}(q_z)F_{kin}(q_z) \quad (2)$$

For $q_z > (q_z)_{crit}$, the specular scattering arising from the specimen's mean electron density profile, $F_{spec}(q_z)$, approaches zero rapidly and monotonically, and thus $|F_{tot}[q_z > (q_z)_{crit}]|^2 \rightarrow\!> |F_{kin}(q_z)|^2$. Therefore, the total meridional x-ray scattering data from these specimens, $I(q_z)$ for $(q_z)_{crit} < (q_z)_{min} \leq q_z \leq (q_z)_{max}$, might be expected to be dominated by the kinematical diffraction arising from the electron density contrast profile, $\Delta\rho(z)$. However, it is important to note here that the maxima contained in this total meridional x-ray scattering, especially for the larger q_z values over this range, could in principle also arise from diffuse scattering due to so-called height-height correlations describing the roughness of the interfaces between the different layers within these specimens. However, our measurements of such diffuse scattering from these specimens, employing both q_x scans perpendicular to q_z as a function of q_z in the plane of the Ewald sphere and more recently "rocking (or q_y) scans" perpendicular to both q_z and the plane of the Ewald sphere as a function of q_z utilizing our area detector, showed that such diffuse scattering is featureless, decaying monotonically with increasing q_z and passes through the minima of the total meridional x-ray scattering for $q_z > 0.05$ Å^{-1}, as shown in Fig. 2. Thus, although its contribution "dominates" the total meridional x-ray scattering for $q_z > 0.05$ Å^{-1}, the maxima of the kinematical x-ray diffraction used for further Fourier analysis as shown in Fig. 3 *a* and obtained from the total meridional x-ray scattering as described in the following paragraph for $q_z > 0.04$ Å^{-1}, do indeed arise from the electron density contrast profile, $\Delta\rho(z)$ (Schlomka et al., 1995; Nitz et al., 1996).

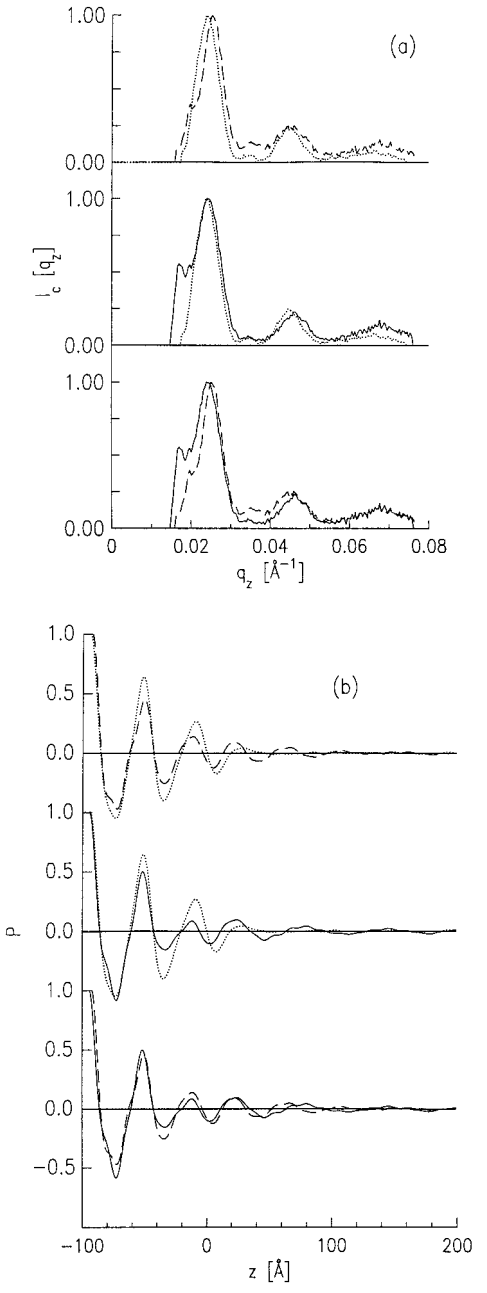

FIGURE 3 Comparisons of relevant pairs of (*a*) corrected meridional intensity functions, $I_c(q_z)$, utilized for subsequent Fourier analysis and (*b*) their respective unique Fourier transforms or Patterson functions, $P(z)$, obtained from the data shown in Fig. 2 as described in the Results, for a typical bare two-unit cell Ge/Si multilayer substrate (· · ·), for the same substrate plus amine-terminated SAM/EMCS linker with self-assembled cytochrome *c* covalently tethered to the surface (- - -), and for cytochrome oxidase self-assembled onto the cytochrome *c* via electrostatic binding (—).

The term $|F_{kin}(q_z)|^2$ for the bare Ge/Si multilayer substrate and the substrate plus each additional overlayer up to the multilayer substrate/SAM/linker/cytochrome *c*/cytochrome oxidase bimolecular complex system was obtained

from the Lorentz-corrected, meridional elastic x-ray scattering, $I_c(q_z)$, by subtraction of the Lorentz-corrected meridional scattering from a uniform silicon substrate (Xu et al., 1993; Murphy et al., 1993). A Lorentz factor of q_z was applied to correct for the ω oscillations of the specimens (Skita et al., 1986). This procedure removed, in effect, both the specular scattering arising from the specimen's mean electron density profile, $|F_{spec}(q_z)|$, and the diffuse scattering arising from interfacial roughness as can be seen from a comparison of Figs. 2 and 3 *a*. In fact, the kinematical diffraction data shown in Fig. 3 *a* obtained in this manner are, indeed, virtually identical for $q_z > 0.04$ Å^{-1} to that obtained directly by subtraction of the diffuse scattering data from the total meridional scattering data shown in Fig. 2. As a result, the kinematical diffraction data subject to further Fourier analysis were restricted to the q_z range $(q_z)_{min} \approx 0.016$ Å$^{-1} \leq q_z \leq (q_z)_{max} \approx 0.076$ Å^{-1} for the protein specimens as shown in Fig. 3 *a*. All Fourier analyses, via both interferometry and holography, were restricted to this q_z window.

The Ge/Si multilayer substrate has very narrow, large-amplitude features in its electron density contrast profile, and its profile structure is essentially known from its fabrication specifications. The addition of the SAM/linker/protein overlayers make a relatively small contribution to the profile structure of the composite system, as their electron density contrast profiles are expected to contain broad, low-amplitude features as compared with those in the profile of the Ge/Si multilayer substrate. The known profile structure of the Ge/Si multilayer substrate can thus be used to determine the profile structure of the SAM/linker/protein overlayers by x-ray interferometry (Lesslauer and Blasie, 1971), as described below. The kinematical meridional x-ray diffraction for the composite structure, as shown in Fig. 2, *b* and *c*, is given by Eq. 3:

$$|F_{kin}(q_z)|^2 = |F_k(q_z)|^2 + |F_u(q_z)|^2 + |F_k(q_z)|\,|F_u(q_z)|\cos\{[\Psi_k(q_z) - \Psi_u(q_z)] + [2\pi q_z A_{ku}]\}, \quad (3)$$

where $|F_{kin}(q_z)|^2$ is the total kinematical structure factor modulus squared of the composite structure and $|F_k(q_z)|^2$ and $|F_u(q_z)|^2$ are the kinematical structure factor moduli squared of the known multilayer substrate and the unknown SAM/linker/protein overlayers, respectively. These three structure factor moduli *could* be obtained experimentally from the kinematical x-ray diffraction from the composite system, from the Ge/Si multilayer substrate itself, and from the SAM/linker/enzyme overlayers on a uniform Si substrate. The terms Ψ_k and Ψ_u are the phases of their respective structure factors, each referenced to the center of mass of their respective profile structures. As the reference profile structure of the Ge/Si multilayer substrate and, therefore, its structure factor, is known, Ψ_k is known. The term Ψ_u is unknown. The term A_{ku} is the distance along the z axis between the centers of mass of the Ge/Si multilayer substrate and the SAM/linker/enzyme overlayers. If the mathematical substitution $\Psi'_u = [\Psi_u - 2\pi q_z A_{ku}]$ is made, then the center of mass of the profile of the unknown overlayer structure is referenced to the center of mass of the profile of the known multilayer reference structure. Solving for the only remaining unknown, Ψ'_u, allows determination of the unknown profile structure of the SAM/linker/protein overlayer. The third term in Eq. 3 represents the critical interference between the strong kinematical diffraction from the Ge/Si multilayer substrate and the weak kinematical diffraction from the SAM/linker/protein overlayer. Its effect can be noted from close inspection of the differences between the meridional x-ray diffraction data of the Ge/Si multilayer substrates (Fig. 2 *a*) and those of the substrates plus SAM/linker/protein(s) shown in Fig. 2, *b* and *c*. However, the interference effects upon addition of the overlayer structures to the Ge/Si multilayer substrate are not especially dramatic for these particular specimens, and therefore, for the purposes of such important comparisons, the data are also shown either as pairs of their corrected meridional intensity functions, $I_c(q_z)$, or as pairs of their respective Fourier transforms, $P(z)$ (i.e., their Patterson functions), in Fig. 3. We note that any disorder in the separation A_{ku} of the SAM/protein overlayer(s) and the multilayer substrate in the profile structures of these composite specimens and/or roughness of the significant interfaces in the profile structure of the overlayer(s) will limit the more obvious manifestation of this interference term to a progressively lower range of q_z, depending on the severity of this disorder and/or roughness. This important result is similarly exhibited via straightforward model calculations in either the kinematical or dynamical diffraction limits upon variation of these relevant parameters. Thus, the more obvious effects of this interference term over the lower q_z range accessible in these experiments (e.g., 0.01 Å$^{-1} < q_z < 0.03$ Å^{-1}) and the more subtle effects of this interference term at larger q_z (>0.03 Å^{-1}), including small changes in amplitudes, positions, and shapes of the diffraction maxima from the multilayer substrate otherwise more dominant in this region are readily evident in Fig. 3 *a*. These experimentally significant interference effects are then appropriately manifest in the inverse Fourier transforms of these data shown in Fig. 3 *b*. The reader is referred to earlier publications from this laboratory concerning the further manifestations of such critical interference effects for a variety of related specimens (especially Xu et al., 1993; Chupa et al., 1994; Prokop et al., 1996; Edwards et al., 1997).

X-ray interferometric analysis of the meridional kinematical x-ray diffraction data was performed utilizing a highly constrained real-space refinement algorithm as described previously (Xu et al., 1991) to accomplish the interferometric phasing of these data. The procedure involved first establishing the relative electron density profile for the "known" Ge/Si multilayer substrate, with the initial models for the substrate being constructed on an absolute electron density scale based on the fabrication specifications. These models were then initially relaxed via a model refinement analysis by comparing the calculated structure factor mod-

ulus squared and its unique Fourier transform (the Patterson function) for the models with their corresponding experimental meridional diffraction data and Patterson functions, subject to the same q_z window as the experimental meridional x-ray diffraction data. Once reasonable (i.e., close but not perfect) agreement had been achieved between the experimental functions and their model counterparts, the constrained real-space refinement algorithm was employed as a final relaxation procedure. The interior portion of the so-refined model relative electron density profile for the bare Ge/Si multilayer substrate (i.e., $Ge_2Si_{30}Ge_2$) was utilized as the primary constraint. This procedure yielded the experimental relative electron density profile for the bare substrate, which exactly predicted both the experimental intensity and Patterson functions. Only the interior portion of this "known" relative electron density profile structure was then used as the reference structure for the constrained real-space refinement of the meridional x-ray diffraction for the multilayer substrate/SAM/linker/protein system because of the modification of the outer silicon layer of the substrate that occurs upon formation of the SAM on its surface by chemisorption (Xu et al., 1993).

The highly constrained real-space refinement algorithm yields one solution to a finite number of possible solutions for the phase of the kinematical structure factor, using the phase dominance of the known reference structure to force the box-refinement algorithm to converge to the local structure most similar to the reference structure (Stroud and Agard, 1979; Makowski, 1981). X-ray holography (Smith, 1969; Lesslauer and Blasie, 1971) was used to prove the correctness of the experimental relative electron density profiles for the composite systems derived via x-ray interferometry. *If* the Ge layers within the reference profile structure of the Ge/Si multilayer substrates are sufficiently narrow (as is possible with MBE fabrication) and A_{ku} is sufficiently large, *then* the unknown profile structure for the SAM/linker/protein overlayer is reconstructed with minimal distortion at the edge of the Patterson function, $P(z)$, which is uniquely obtained by Fourier transformation of the kinematical meridional x-ray diffraction data without any phase information.

Fig. 4 summarizes the various stages in the determination of the correct profile structure of self-assembled cytochrome *c* tethered to a multilayer substrate via the amine-terminated SAM and the EMCS linker. Fig. 4 *b* shows the experimental relative electron density profile structure, $\Delta\rho_{exp}(z)$, for the composite Ge/Si multilayer substrate/SAM/linker/cytochrome *c* system, derived by applying the constrained real-space refinement to the specimen's meridional x-ray diffraction data using the reference structure as the primary constraint. The two sharpest peaks of high density correspond to the Ge_2 layers in the multilayer substrate. To understand the nature and source of the additional features, a real-space model on an absolute electron density scale was constructed to account for each feature. Fig. 4 *d* shows the refined model absolute electron density profile, $\rho_{mod}(z)$, for the Ge/Si multilayer substrate/amine SAM/EMCS linker/cytochrome *c* system, which accounts for each feature in $\Delta\rho_{exp}(z)$ (Fig. 4 *b*). This fact is demonstrated by a comparison of Fig. 4 *b* with Fig. 4 *c*, the model relative electron density profile, $\Delta\rho_{mod}(z)$, where $\Delta\rho_{mod}(z)$ is uniquely calculated by a double Fourier transform (i.e., Fourier transform-inverse Fourier transform) of $\rho_{mod}(z)$ subject to the experimental q_z window. A one-to-one correspondence between each feature in the refined model relative electron density profile and its counterpart in the experimental relative electron density profile established both the position (± 0.1 Å) and electron density level (± 0.01 electrons/Å^3) of each feature in the so-refined $\rho_{mod}(z)$ (Murphy et al., 1993).

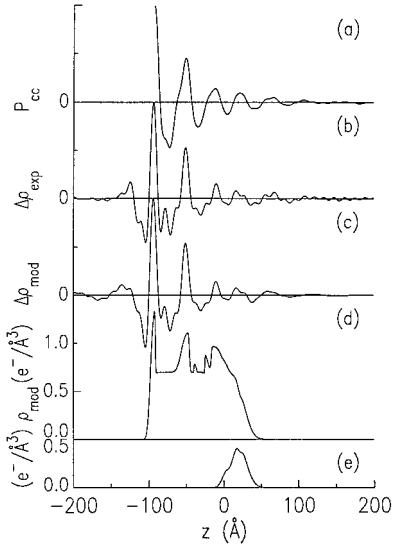

FIGURE 4 (*a*) Experimental Patterson function, P_{cc}, for the self-assembled cytochrome *c* system. The origin has been offset horizontally to correspond with the first Ge peak in $\Delta\rho_{exp}$ for ease of comparison. (*b*) Experimental relative electron density profile, $\Delta\rho_{exp}$, for the cytochrome *c* system. (*c*) Refined model relative electron density profile, $\Delta\rho_{mod}$, for the cytochrome *c* system. (*d*) Refined model absolute electron density, ρ_{mod}, for the cytochrome *c* system in units of $e^-/Å^3$. (*e*) Estimated cytochrome *c* contribution to the refined model absolute electron density shown in *d*. See text for additional details.

The previously mentioned peak features corresponding to the Ge layers in the substrate are positioned at $z \approx -93$ Å and $z \approx -49$ Å in Fig. 4 *d*. Regions between the Ge peaks having an electron density of 0.7 electrons/Å^3 represent the silicon layers. After the formation of only the amine SAM on the surface of the substrate, analysis of the x-ray diffraction data at this stage (not shown) indicates considerable Ge migration toward the substrate's surface. This kind of substrate evolution has been reported previously (Murphy et al., 1993; Edwards et al., 1997) for MBE substrates alkylated by the Sagiv liquid-phase method (Sagiv, 1980) but is more marked in this case, presumably due to the high annealing temperature required by the vapor-phase silanization. We note that only the nearly constant interior $Ge_2Si_{30}Ge_2$ portion of the MBE multilayer substrate was used as the reference structure in our determination of these profile struc-

tures to minimize any possible adverse effects due to the evolution of the Ge_2Si_{30} surface of these substrates during subsequent chemisorption and/or physisorption on their surfaces. Analysis after addition of the EMCS linker to the SAM (not shown) shows a continuation of this substrate evolution, which is evidenced by the small, sharp peaks at $z \approx -39$ Å and $z \approx -25$ Å and the broader peak at $z \approx -14$ Å in Fig. 4 *d*. Unfortunately, this large peak close to the surface of the MBE substrate (at $z \approx 0$ Å) somewhat masks the contribution from the cytochrome *c*, which is seen only as a broadening of this peak with shoulders at $z \approx 2$ Å, 16 Å, and 25 Å. However, by subtraction of the absolute electron density profile of this sample immediately before incubation in the cytochrome *c* (i.e., the absolute electron density profile for the substrate/SAM/linker system) we can obtain a good estimate of the profile contribution due to the protein as shown in Fig. 4 *e*. Aside from a minor variation within the substrate nearest its surface ($z < 0$ Å), we see a nearly symmetrical feature occurring within $0 < z < 50$ Å with a full-width-at-half-maximum (FWHM) of ~30 Å. We note here that the addition of this cytochrome *c* feature within $0 < z < 50$ Å, as described, is sufficient to result in a good match of $\Delta\rho_{mod}(z)$ to $\Delta\rho_{exp}(z)$ for $z > 50$ Å; thus the features in $\Delta\rho_{exp}(z > 50$ Å) arise from [low-frequency $(q_z)_{min}$, high-frequency $(q_z)_{max}$] Fourier transform truncation effects only. The criteria for x-ray holography (Smith, 1969; Lesslauer and Blasie, 1971) are satisfied for the SAM/linker/cytochrome *c* system, and therefore the experimental electron density profile can be proven to be correct. Fig. 4 *a* is the Patterson function, $P_{cc}(z)$, for $z \geq 0$ for the SAM/linker/cytochrome *c* system (the origin of which has been offset horizontally to correspond with the first Ge_2 peak in $\Delta\rho_{exp}(z)$ for ease of comparison). Comparison of the features in Fig. 4, *a* and *b*, over the region 0 Å $\leq z \leq 50$ Å reveals that the Ge_2 peak feature at the left edge of the relative electron density profile is convoluted with the SAM/linker/cytochrome *c* overlayer features at the right edge of the profile to reconstruct these same features in the Patterson function over the same region of *z*. Therefore, the nearly identical agreement between the SAM/linker/cytochrome *c* overlayer profile features at the edge of the Patterson function and those at the edge of the relative electron density profile indicates that the organic overlayer profile structure derived via x-ray interferometry is proven correct by x-ray holography.

Similarly, Fig. 5 summarizes the various stages in the determination of the correct profile structure of the system with self-assembled cytochrome oxidase bound to the cytochrome *c*. Fig. 5 *b* shows the experimental relative electron density profile structure, $\Delta\rho_{exp}(z)$, for the composite Ge/Si multilayer substrate/SAM/linker/cytochrome *c*/cytochrome oxidase system, derived as indicated above. The two peaks corresponding to the Ge_2 layers in the multilayer substrate are still clearly evident, as is the cytochrome *c* contribution occurring in the range 0 Å $\leq z \leq 50$ Å, but now there are additional features beyond 50 Å from the surface. Again, a real-space model on an absolute electron density scale was constructed to account for each additional feature. Fig. 5 *d* shows the refined model absolute electron density profile, $\rho_{mod}(z)$, for the Ge/Si multilayer substrate/amine SAM/linker/cytochrome *c*/cytochrome oxidase system, which accounts for each feature in $\Delta\rho_{exp}(z)$ (Fig. 5 *b*). A comparison of Fig. 5 *b* with Fig. 5 *c* (the model relative electron density profile, $\Delta\rho_{mod}(z)$, obtained as outlined above) shows a one-to-one correspondence between each feature establishing both the position (±0.1 Å) and electron density level (±0.01 $e^-/Å^3$) of each feature in the so-refined absolute electron density profile (Fig. 5 *d*).

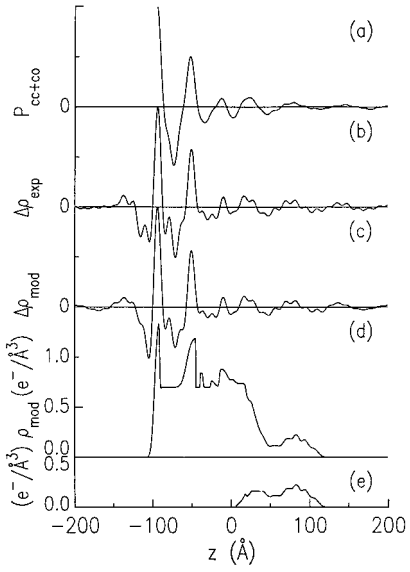

FIGURE 5 (*a*) Experimental Patterson function, P_{cc+co}, for the bimolecular complex system of cytochrome *c* plus cytochrome oxidase. The origin has been offset horizontally to correspond with the first Ge peak in $\Delta\rho_{exp}$ for ease of comparison. (*b*) Experimental relative electron density profile, $\Delta\rho_{exp}$, for the bimolecular complex system. (*c*) Refined model relative electron density profile, $\Delta\rho_{mod}$, of the bimolecular complex system. (*d*) Refined model absolute electron density, ρ_{mod}, for the bimolecular complex system in units of $e^-/Å^3$. (*e*) Estimated cytochrome oxidase contribution to the refined model absolute electron density shown in *d*. See text for additional details.

The migrating germanium peaks at $z \approx -39$ Å, $z \approx -25$ Å, and $z \approx -14$ Å are still evident in Fig. 5 *d*, although their electron densities have altered slightly. There also appears to be some change in the region 0 Å $\leq z \leq 50$ Å ascribed to the covalently tethered cytochrome *c* monolayer before cytochrome oxidase binding, but the most dramatic change is the addition of a region of electron density spanning the range 50 Å $\leq z \leq 120$ Å that was not previously present. Once again, by subtraction of the absolute electron density profile of the substrate/SAM/linker/cytochrome *c* system, we can obtain a first estimate (see Discussion) of the profile contribution due to the addition of the cytochrome oxidase as shown in Fig. 5 *e*. This profile spans the range 5 Å $< z <$ 125 Å and consists of two regions of higher electron density (centered at $z \approx 83$ Å and $z \approx 33$ Å) separated by a region of lower electron density centered at $z \approx 55$ Å. We note here that the addition of this cytochrome oxidase feature, as

described, is both necessary to provide a good match of $\Delta\rho_{mod}(z)$ to $\Delta\rho_{exp}(z)$ for 5 Å $< z <$ 125 Å and sufficient to result in a good match of $\Delta\rho_{mod}(z)$ to $\Delta\rho_{exp}(z)$ for $z >$ 125 Å; thus these latter features in $\Delta\rho_{exp}(z >$ 125 Å) arise from [low-frequency $(q_z)_{min}$, high-frequency $(q_z)_{max}$] Fourier transform truncation effects only. The criteria for x-ray holography (Smith, 1969; Lesslauer and Blasie, 1971) are also satisfied for the SAM/linker/cytochrome *c*/cytochrome oxidase system, and therefore the experimental electron density profile can be proven to be correct. Fig. 5 *a* is the Patterson function, $P_{cc+co}(z)$, for $z \geq 0$ for the SAM/linker/cytochrome *c*/cytochrome oxidase system (the origin of which has been offset horizontally to correspond with the first Ge_2 peak in $\Delta\rho_{exp}(z)$ for ease of comparison). Comparison of the features in Fig. 5, *a* and *b*, over the region 50 Å $\leq z \leq$ 120 Å reveals that the Ge_2 peak feature at the left edge of the relative electron density profile is convoluted with the SAM/linker/cytochrome *c*/cytochrome oxidase overlayer features at the right edge of the profile to reconstruct these same features in the Patterson function over the same region of *z*. Therefore, the nearly identical agreement between the SAM/linker/cytochrome *c*/cytochrome oxidase overlayer profile features at the edge of the Patterson function and those at the edge of the relative electron density profile indicates that the organic overlayer profile structure derived via x-ray interferometry is proven correct by x-ray holography.

DISCUSSION

Cytochrome *c* can be considered (for our purpose here) to possess a spherical envelope of approximately 31 Å diameter and, thus, in a densely packed hexagonal array the number of molecules in a monolayer would be 1.2×10^{13} cm^{-2} (Steinemann and Läuger, 1971) resulting in a maximal surface concentration of 20.0 nM for a monolayer, only two-thirds of our experimental value. However, if the heme planes of the cytochrome *c* are not randomly oriented and are instead somehow oriented with respect to the substrate plane, then the extinction coefficient for a solution is no longer applicable. Previous studies on yeast cytochrome *c* monolayers covalently bound to a surface have shown the protein molecules to be oriented with their average heme plane more parallel than perpendicular to the substrate plane (Pachence at al., 1990). In the limit that all of the heme planes are parallel to the monolayer plane, the extinction coefficient for the oriented hemes will be one and a half times that of the solution value, thus making our observed absorbance consistent with exactly one close-packed monolayer. The reality based only on such optical absorption results is, therefore, likely to be somewhere between the two extremes of a close-packed monolayer and one and a half monolayers. From work on similar systems (Pachence at al., 1990; Edwards and Blasie, unpublished data) we expect the cytochrome *c* to orient with its heme planes more parallel than perpendicular to the substrate plane, but we have also frequently observed the tendency of yeast cytochrome *c* to dimerize, a tendency we were hoping to decrease by soaking the samples in the 1 mM dithiothreitol. Indeed, we observed little to no evidence of multilayer formation in the electron density profiles for the cytochrome *c* overlayer (see below).

The cytochrome oxidase concentration of 5.6 nM is similar to that previously observed by this group (Edwards et al., 1997) for monolayers of cytochrome oxidase self-assembled on amine-terminated SAMs that were designed to mimic the lysine residues of cytochrome *c* that are known to be involved in the binding of this protein to cytochrome oxidase. This surface concentration corresponds to an average area per molecule in the monolayer plane of 2964 $Å^2$. Valpuesta et al. (1990) reported unit cell dimensions of $a =$ 102 Å, $b =$ 123 Å, with two dimers per unit cell for their frozen, hydrated two-dimensional crystals, whereas Frey and Murray (1994) reported unit cell dimensions of $a =$ 95 Å, $b =$ 123 Å for similarly prepared two-dimensional crystals having the same space group. These dimensions result in areas per molecules of 3137 $Å^2$ and 2921 $Å^2$, respectively. Hence, we can estimate that we have approximately a single, densely packed monolayer of cytochrome oxidase. In our previous study (Edwards et al., 1997) the average heme plane was found to be more perpendicular than parallel to the substrate plane. In the limit that all of the heme planes were perpendicular to the substrate, this would reduce the extinction coefficient to three-fourths of its solution value and result in an average area per molecule of 2223 $Å^2$. However, the electron density profile for the cytochrome oxidase overlayer indicates that the oxidase molecules are oriented with their long axes substantially tilted with respect to the normal to the substrate plane (see below).

The formation of cytochrome *c*/cytochrome oxidase bimolecular complex films on MBE substrates allowed the determination of the profile structure of the system by x-ray interferometry, and proof of the correctness of these so-derived profile structures by x-ray holography, to a spatial resolution of ~12 Å as estimated from the wavelength of the high frequency $(q_z)_{max}$ truncation ripple in Fig. 5 *b*. Figs. 6 *a* and 7 *a* show the experimental absolute electron density profiles for the MBE/SAM/linker/cytochrome *c* and the MBE/SAM/linker/cytochrome *c*/cytochrome oxidase systems, respectively. These were obtained by summation of the mean electron density profile for the refined model absolute electron density profile, $\bar{\rho}_{mod}(z)$, and the experimental relative electron density profile, $\Delta\rho_{exp}(z)$ (see Eq. 1). This procedure eliminates any $(q_z)_{min}$ truncation effects from the experimental electron density profile, leaving only the high spatial frequency components, due to the $(q_z)_{max}$ truncation, in the profile. Figs. 6 *b* and 7 *b* show the corresponding refined model absolute electron density profiles for comparison. First, this comparison demonstrates that a smooth variation in electron density through the mean of the $(q_z)_{max}$ truncation ripple between -50 Å $< z <$ 0 Å in Figs. 6 *a* and 7 *a* might better represent physically the distribution of migrated Ge within the silicon surface layer

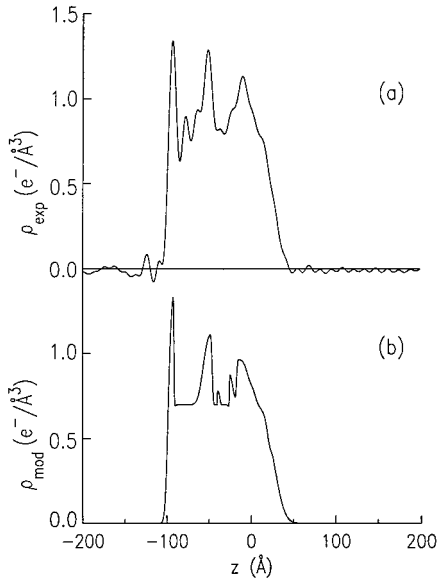

FIGURE 6 (*a*) Experimental absolute electron density profile for the self-assembled cytochrome *c* specimen, produced by summation of the mean electron density profile, $\bar{\rho}_{mod}$ (*z*), with the experimental relative electron density profile, $\Delta\rho_{exp}$ (*z*), to contain only $(q_z)_{max}$ truncation effects. (*b*) Refined model absolute electron density, ρ_{mod} (*z*), for the cytochrome *c* specimen.

of these substrates than the discrete layers in the model profiles of Figs. 6 *b* and 7 b, respectively. More importantly, in a previous study of cytochrome oxidase self-assembled onto an amine-terminated SAM (Edwards et al., 1997), the experimental absolute electron density profile was compared with the low-resolution three-dimensional structure for the oxidase molecule obtained from the electron microscopy of a two-dimensional crystalline form of the oxidase (Valpuesta et al., 1990), a form more similar to these single monolayers than that of the three-dimensional crystalline form. Although the two profiles were very similar, the shorter profile length observed for the self-assembled monolayer, combined with experimental optical linear dichroism results indicated some degree of tilting of the long axis of the cytochrome oxidase with respect to the normal to the substrate plane. Fig. 8 shows a comparison of the protein overlayer regions of the experimental absolute electron density profiles for cytochrome oxidase self-assembled directly onto an amine-terminated SAM (Edwards et al., 1997) (Fig. 8 *b*) and self-assembled onto a cytochrome *c* monolayer in the current study (Fig. 8 *c*). The cytochrome oxidase profile in Fig. 8 *b* has been offset to the right for ease of comparison because, being tethered to the substrate surface by only an amine-terminated SAM, the position of this feature was originally closer to the substrate surface. However, in the range shown, the two experimental absolute electron density profiles can be seen to be quite similar in shape and width. The profile for the cytochrome oxidase in the bimolecular complex is somewhat higher in electron density and

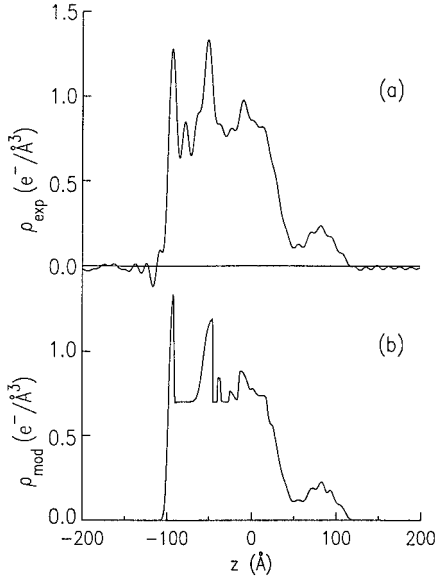

FIGURE 7 (*a*) Experimental absolute electron density profile for the bimolecular complex of cytochrome *c*/cytochrome oxidase, produced by summation of the mean electron density profile, $\bar{\rho}_{mod}$ (*z*), with the experimental relative electron density profile, $\Delta\rho_{exp}$ (*z*), to contain only $(q_z)_{max}$ truncation effects. (*b*) Refined model absolute electron density, ρ_{mod} (*z*), for the cytochrome *c*/cytochrome oxidase specimen.

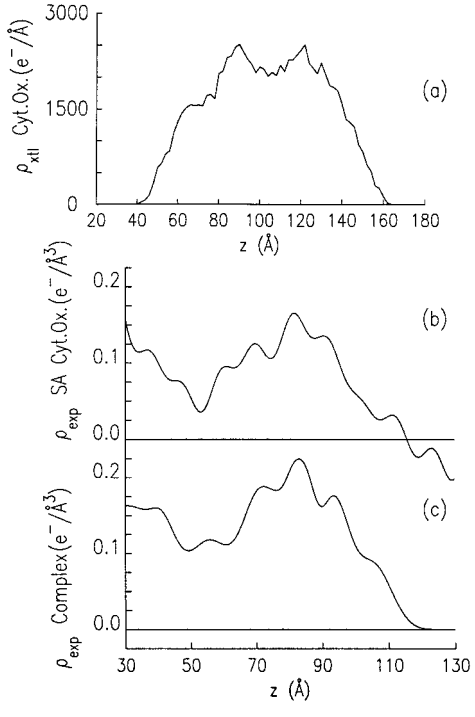

FIGURE 8 (*a*) Projection onto the long axis of the cytochrome oxidase molecule of the integration (over the planes perpendicular to this axis) of the electron density of one unidirectional dimer of cytochrome oxidase as obtained from the x-ray crystallographic data. (*b*) Expanded protein overlayer portion of the experimental absolute electron density profile obtained for a self-assembled cytochrome oxidase monolayer specimen (Edwards et al., 1997). (*c*) Expanded protein overlayer portion of the experimental absolute electron density profile obtained for the cytochrome *c*/cytochrome oxidase bimolecular complex. See text for additional details.

possibly slightly narrower in width, indicating that slightly more cytochrome oxidase self-assembled to the cytochrome *c* surface than the simple amine-terminated SAM surface (in agreement with optical spectroscopy results) and that the cytochrome oxidase in the bimolecular complex may have, on average, its long axis even more tilted with respect to the normal to the substrate plane than found for cytochrome oxidase directly bound to the SAM. We also observe that the cytochrome oxidase profile for the bimolecular complex in Fig. 8 *c* is not quite as asymmetric as that shown in Fig. 8 *b*. This is understandable, as in the bimolecular complex, the cytochrome oxidase is connected to the MBE substrate via several "soft" interfaces (i.e., the SAM, EMCS linker and cytochrome *c*) leading to the possibility of a greater spread of cytochrome oxidase positions in the profile *z* direction and, therefore, a broadening of the profile features relative to those of Fig. 8 *b*. For comparison, Fig. 8 *a* shows the projection onto the long axis of the cytochrome oxidase molecule of the integration (over the planes perpendicular to this axis) of the electron density of one unidirectional dimer of cytochrome oxidase as obtained from the x-ray crystallographic data (Tsukihara et al., 1996). Hence, this plot is analogous to what we see from x-ray interferometry except, in this case, the molecule is not tilted and therefore has a broader profile width. Indeed, the *z* axis scales are not the same for Fig. 8 *a* and Fig. 8, *b* and *c*, but rather the profiles are displayed so as to give the best visual comparison. The projected electron density of the crystal (Fig. 8 *a*) can be seen to be strikingly similar to the cytochrome oxidase portion of the experimental absolute electron density profiles, especially that for the self-assembled cytochrome oxidase monolayer shown in Fig. 8 *b*.

The disorder at the interfaces means that the precise endpoint of either the cytochrome *c* or the cytochrome oxidase contribution to the bimolecular complex electron density profile is hard to ascertain due to the absence of deep minima between the component contributions. The difference profile shown in Fig. 4 *e* (obtained by subtraction of the absolute electron density profile of this sample immediately before incubation in the cytochrome *c*) as a measure of the cytochrome *c* contribution alone is consistent in general shape with electron density profiles obtained by others either experimentally (Amador et al., 1993; Chupa et al., 1994) or theoretically (Chupa et al., 1994; Tobias et al., 1996) for yeast cytochrome *c* covalently tethered to a SAM. Electron density profiles from computer simulations (Tobias et al., 1996) indicated the profile width to be ~20 Å with an electron density of nearly 0.5 $e^-/Å^{-3}$. Experimentally derived profiles (Chupa et al., 1994) obtained this maximal electron density but showed a slightly broadened profile width due to the inherent disorder of the SAM endgroup (sulfhydryl) surface to which the protein was directly tethered. In the current study, the maximal electron density is somewhat less, being just over 0.4 $e^-/Å^{-3}$, and the profile is significantly broadened at the edges so that the profile FWHM value increases to ~25 Å. This indicates an even greater disorder of the tethering endgroup surface as would be expected for such indirect tethering of the protein to the SAM endgroups via the EMCS linker, resulting in a more loose tethering of the protein.

A first estimate of the contribution made by the cytochrome oxidase (obtained by subtraction of the absolute electron density profile of this sample after incubation in just cytochrome *c*) was given in the difference profile of Fig. 5 *e*. This profile contains two regions of higher electron density separated by a small region of lower electron density. As better shown in Fig. 9, the region of higher electron density furthest from the substrate (50 Å $< z <$ 150 Å) appears to be consistent with the previously obtained profile of cytochrome oxidase (Edwards et al., 1997), as shown in Fig. 8 *b*. However, these previous results did not indicate another region of high electron density closer to the substrate (5 Å $< z <$ 50 Å). This region overlaps with the profile position of cytochrome *c* before the binding of cytochrome oxidase, as indicated in Fig. 4 *e*. In fact, comparison of the tethered cytochrome *c* profile with that after binding of cytochrome oxidase (Fig. 9) for 0 Å $< z <$ 50 Å suggests that the profile width of the cytochrome *c* feature simply increases by ~10 Å upon cytochrome oxidase binding, and hence we theorize that a change in profile position and/or orientation of some fraction of the cytochrome *c* occurs upon the electrostatic binding of the cytochrome oxidase, thus further broadening the contribution of cytochrome *c* to the overall absolute electron density profile. It is interesting to note in this regard that the actual molecular envelope of cytochrome *c* is a prolate ellipsoid (25 Å × 25 Å × 35 Å). The long axis is parallel to the substrate plane before interaction with the cytochrome oxidase, as described previously (Chupa et al., 1994). Thus, rotation of the covalently tethered cytochrome *c* molecules upon interac-

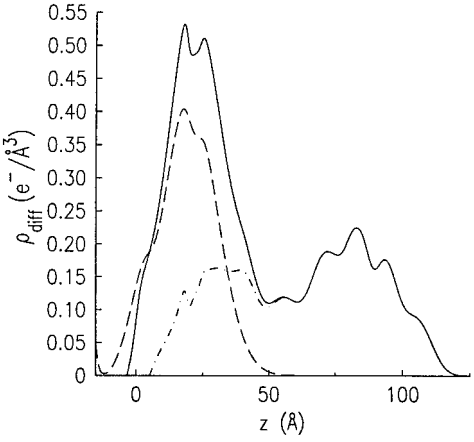

FIGURE 9 Absolute electron density profiles for yeast cytochrome *c* covalently tethered to an amine-terminated SAM surface via the EMCS linker (- - -) and for cytochrome oxidase self-assembled onto the sotethered cytochrome *c* monolayer's surface via electrostatic binding (—), together with the difference between these two profiles (- · - for $z <$ 50 Å and — for $z >$ 50 Å). The difference profile for 5 Å $< z <$ 50 Å (- · -) suggests a perturbation of the cytochrome *c* monolayer profile induced by the electrostatic binding of the oxidase (see text for additional details).

tion with the cytochrome oxidase so that their long axes are now more normal to the substrate plane would itself be sufficient to explain the ~10-Å broadening of the cytochrome *c* feature. Such a large rotation seems plausible when employing here the more loose tethering of the yeast cytochrome *c* to the SAM endgroups indirectly via the EMCS linker, especially considering that molecular dynamics simulations (Tobias et al., 1996) showed that rotations of 30° are possible with the tighter tethering of the protein directly to the endgroups.

CONCLUSIONS

We have demonstrated, monolayer by monolayer, the sequential formation via self-assembly of the bimolecular complex between cytochrome *c* and cytochrome *c* oxidase vectorially oriented at the soft interface provided by an organic SAM chemisorbed onto the surface of a solid inorganic substrate. The fabrication of these self-assembled films on MBE substrates allowed the determination of the profile structure of the system by x-ray interferometry, and proof of the correctness of these so-derived profile structures by x-ray holography, at each stage of the sequential fabrication process. The profile structure of cytochrome *c* covalently tethered via the EMCS linker to the SAM's surface is slightly broader than that for the protein covalently tethered directly to a SAM's surface. The electrostatic binding of its natural electron acceptor, cytochrome oxidase, to the so-tethered cytochrome *c* monolayer occurs more than an order of magnitude faster than that for the binding of cytochrome oxidase directly to an amine-terminated SAM meant to mimic the surface lysine residues of cytochrome *c*. Although the profile structures of each membrane protein within the bimolecular complex were qualitatively similar to those for each protein tethered separately to an appropriate SAM endgroup surface, the cytochrome *c* profile was substantially affected by the electrostatic binding of the oxidase, consistent with a displacement and/or reorientation of a substantial fraction of the cytochrome *c* molecules. These vectorially oriented monolayers of the bimolecular complex are now sufficiently well characterized structurally to undertake a number of more definitive functional studies.

A. M. Edwards especially thanks Prof. Takashi Yonetani for his guidance during the cytochrome oxidase preparation.

This work was supported by National Institutes of Health grant GM33525 to J. K. Blasie.

REFERENCES

Amador, S. M., J. M. Pachence, R. Fischetti, J. P. McCauley, Jr., A. B. Smith, III, and J. K. Blasie. 1993. Use of self-assembled monolayers to covalently tether protein monolayers to the surface of solid substrates. *Langmuir*. 9:812–817.

Asturias, F. J., R. F. Fischetti, and J. K. Blasie. 1994. Changes in the profile structure of the sarcoplasmic reticulum membrane induced by phosphorylation of the Ca^{2+}-ATPase enzyme in the presence of terbium: a time-resolved x-ray diffraction study. *Biophys. J.* 66:1653–1664.

Bean, J. C., L. C. Feldman, A. T. Fiory, S. Nakahara, and I. K. Robinson. 1984. Ge_xSi_{1-x}/Si strained-layer superlattice grown by molecular beam epitaxy. *J. Vac. Sci. Technol*. A2:436–440.

Blasie, J. K., S. Xu, M. Murphy, J. Chupa, J. P. McCauley, Jr., A. B. Smith, III, L. J. Peticolas, and J. C. Bean. 1992. Profile structures of macromolecular monolayers on solid substrates by x-ray interferometry/holography. *Materials Res. Soc. Symp. Proc*. 237:399–409.

Chupa, J. A., J. P. McCauley, Jr., R. M. Strongin, A. B. Smith, III, J. K. Blasie, L. J. Peticolas, and J. C. Bean. 1994. Vectorially oriented membrane protein monolayers: profile structures via x-ray interferometry/holography. *Biophys. J* 67:336–348.

Collinson, M., E. F. Bowden, and M. J. Tarlov. 1992. Voltammetry of covalently immobilized cytochrome *c* on self-assembled monolayer electrodes. *Langmuir*. 8:1247–1250.

Cowley, J. M. 1981. Diffraction Physics, 2nd ed. North-Holland Publishing Co., Amsterdam. 430 pp.

Cullinson, J. K., F. M. Hawkridge, N. Nakashima, and S. Yoshikawa. 1994. A study of cytochrome *c* oxidase in lipid bilayer membranes on electrode surfaces. *Langmuir*. 10:877–882.

Dickinson, L. C., and J. C. W. Chien. 1975. Cobalt-cytochrome *c*. I. Preparation, properties and enzymic activity. *Biochemistry*. 14: 3526–3534.

Edwards, A. M., J. A. Chupa, R. M. Strongin, A. B. Smith, III, and J. K. Blasie. 1997. Vectorially-oriented monolayers of cytochrome oxidase: fabrication and profile structures. *Langmuir*. 13:1634–1643.

Frey, T. G., and J. M. Murray. 1994. Electron microscopy of cytochrome *c* oxidase crystals. *J. Mol. Biol.* 237:275–297.

Guo, L.-H., G. McLendon, H. Razafitrimo, and Y. Gao. 1996. Photo-active and electro-active protein films prepared by reconstitution with metalloporphyrins self-assembled on gold. *J. Materials Chem.* 6:369–374.

Hong, H.-G., M. Jiang, S. G. Sligar, and P. W. Bohn. 1994. Cysteine-specific surface tethering of genetically engineered cytochromes for fabrication of metalloprotein nanostructures. *Langmuir*. 10:153–158.

Jiang, M., B. Nolting, P. S. Stayton, and S. G. Sligar. 1996. Surface-linked molecular monolayers of an engineered myoglobin: structure, stability, and function. *Langmuir*. 12:1278–1283.

Lesslauer, W., and J. K. Blasie. 1971. X-ray holographic interferometry in the determination of planar multilayer structures: theory and experimental observations. *Acta Crystallogr*. A27:456–461.

Makowski, L. 1981. The use of continuous diffraction data as a phase constraint. I. One-dimensional theory. *J. Appl. Crystallogr*. 14:160–168.

Malatesta, F., G. Antonini, F. Nicoletti, A. Giuffrè, E. D'itri, P. Sarti, and M. Brunori. 1996. Probing the high-affinity site of beef heart cytochrome *c* oxidase by cross-linking. *Biochem. J.* 315:909–916.

Murphy, M. A., J. K. Blasie, L. J. Peticolas, and J. C. Bean. 1993. X-ray interferometry/holography for the unambiguous determination of the profile structures of single Langmuir-Blodgett monolayers. *Langmuir*. 9:1134–1141.

Nitz, V., M. Tolan, J.-P. Schlomka, O. H. Seeck, J. Stettner, and W. Press. 1996. Correlations in the interface structure of Langmuir-Blodgett films observed by x-ray scattering. *Phys. Rev. B.* 54:5038–5050.

Okunuki, K., I. Sekuzu, T. Yonetani, and S. Takemori. 1958. Studies on cytochrome a. I. Extraction, purification and some properties of cytochrome a. *J. Biochem. (Tokyo).* 45:847–854.

Owaku, K., M. Goto, Y. Ikariyama, and M. Aizawa. 1995. Protein A Langmuir-Blodgett film for antibody immobilization and its use in optical immunosensing. *Anal. Chem.* 67:1613–1616.

Pachence, J. M., S. Amador, G. Maniara, J. Vanderkooi, P. L. Dutton, and J. K. Blasie. 1990. Orientation and lateral mobility of cytochrome *c* on the surface of ultrathin lipid multilayer films. *Biophys. J.* 58:379–389.

Pachence, J. M., R. F. Fischetti, and J. K. Blasie. 1989. Location of the heme-Fe atoms within the profile structure of a monolayer of cytochrome *c* bound to the surface of an ultrathin lipid multilayer film. *Biophys. J.* 56:327–337.

Prokop, L. A., R. M. Strongin, A. B. Smith, III, J. K. Blasie, L. J. Peticolas, and J. C. Bean. 1996. Vectorially oriented monolayers of detergent-

solubilized Ca^{2+}-ATPase from sarcoplasmic reticulum. *Biophys. J.* 70: 2131–2143.

Rabanal, F., B. R. Gibney, W. F. DeGrado, C. C. Moser, and P. L. Dutton. 1996. Engineering photosynthesis: synthetic redox proteins. *Inorg. Chim. Acta*. 243:213–218.

Robertson, D. E., R. S. Farid, C. C. Moser, J. L. Urbauer, S. E. Mulholland, R. Pidikiti, J. D. Lear, A. J. Wand, W. F. DeGrado, and P. L. Dutton. 1994. Design and synthesis of multi-haem proteins. *Nature*. 368: 425–432.

Sagiv, J. 1980. Organized monolayers by adsorption. I. Formation and structure of oleophobic mixed monolayers on solid surfaces. *J. Am. Chem. Soc*. 102:92–98.

Schlomka, J.-P., M. Tolan, L. Schwalowsky, O. H. Seeck, J. Stettner, and W. Press. 1995. X-ray diffraction from Si/Ge layers: diffuse scattering in the region of total external reflection. *Phys. Rev. B.* 51:2311–2321.

Skita, V., M. Filipkowski, A. F. Garito, and J. K. Blasie. 1986. Profile structures of very thin multilayers by x-ray diffraction using direct refinement methods of analysis. *Phys. Rev. B.* 34:5826–5837.

Smith, H. M. 1969. Principles of Holography. Wiley-Interscience, New York. 239 pp.

Song, S., R. A. Clark, E. F. Bowden, and M. J. Tarlov. 1993. Characterization of cytochrome *c*/alkanethiolate structures prepared by self-assembly on gold. *J. Phys. Chem.* 97:6564–6572.

Steinemann, A., and P. Läuger. 1971. Interaction of cytochrome *c* with phospholipid monolayers and bilayer membranes. *J. Membr. Biol.* 4:74–86.

Stroud, R. M., and D. A. Agard. 1979. Structure determination of asymmetric membrane profiles using an iterative Fourier method. *Biophys. J.* 25:495–512.

Tobias, D. J., W. Mar, J. K. Blasie, and M. L. Klein. 1996. Molecular dynamics simulations of a protein on hydrophobic and hydrophilic surfaces. *Biophys. J.* 71:2933–2941.

Tsukihara, T., H. Aoyama, E. Yamashita, T. Tomizaki, H. Yamaguchi, K. Shizawa-Itoh, R. Nakashima, R. Yaono, and S. Yoshikawa. 1996. The whole structure of the 13-subunit oxidized cytochrome c oxidase at 2.8 Å. *Science*. 272:1136–1144.

Valpuesta, J. M., R. Henderson, and T. G. Frey. 1990. Electron cryomicroscopic analysis of crystalline cytochrome oxidase. *J. Mol. Biol.* 214:237–251.

Xu, S., R. F. Fischetti, J. K. Blasie, L. J. Peticolas, and J. C. Bean. 1993. Profile and in-plane structures of self-assembled monolayers on Ge/Si multilayer substrates by high-resolution x-ray diffraction employing x-ray interferometry/holography. *J. Phys. Chem*. 97:1961–1969.

Xu, S., M. A. Murphy, S. M. Amador, and J. K. Blasie. 1991. Proof of asymmetry in the Cd-arachidate bilayers of ultrathin Langmuir-Blodgett multilayer films via x-ray interferometry. *J. Phys. I.* 1:1131–1144.

Yonetani, T. 1960. Studies on cytochrome oxidase. I. Absolute and difference absorption spectra. *J. Biol. Chem.* 235:845–852.

Yonetani, T. 1961. Studies on cytochrome oxidase. III. Improved preparation and some properties. *J. Biol. Chem.* 236:1680–1688.

Zaslavsky, D. L., I. A. Smirnova, S. A. Siletsky, A. D. Kaulen, F. Millet, and A. A. Konstantinov. 1995. Rapid kinetics of membrane potential generation by cytochrome *c* oxidase with the photoactive Ru(II)-tris-bipyridyl derivative of cytochrome *c* as electron donor. *FEBS Lett*. 359:27–30.

Zhang, K., A. M. Edwards, J. Dong, J. Chupa, and J. K. Blasie. 1997. XAFS on vectorially oriented single monolayer protein samples. *J. Phys. IV*. C2:593–597.